OPEN ACCESS
IOP Publishing
Classical and Quantum Gravity
Class. Quantum Grav. **37** (2020) 095004 (20pp)
https://doi.org/10.1088/1361-6382/ab77e9

Amorphous optical coatings of present gravitational-wave interferometers*

M Granata[1,5], A Amato[1], L Balzarini[1,6], M Canepa[2,3], J Degallaix[1], D Forest[1], V Dolique[1,7], L Mereni[1], C Michel[1], L Pinard[1], B Sassolas[1], J Teillon[1] and G Cagnoli[4]

[1] Laboratoire des Matériaux Avancés-IP2I, CNRS, Université de Lyon, F-69622 Villeurbanne, France
[2] OPTMATLAB, Dipartimento di Fisica, Università di Genova, Via Dodecaneso 33, 16146 Genova, Italy
[3] INFN, Sezione di Genova, Via Dodecaneso 33, 16146 Genova, Italy
[4] Université de Lyon, Université Claude Bernard Lyon 1, CNRS, Institut Lumiére Matiére, F-69622, Villeurbanne, France

E-mail: m.granata@lma.in2p3.fr

Received 19 September 2019, revised 8 January 2020
Accepted for publication 19 February 2020
Published 2 April 2020

Abstract

We report on the results of an extensive campaign of optical and mechanical characterization of the ion-beam sputtered oxide layers (Ta_2O_5, TiO_2, Ta_2O_5–TiO_2, SiO_2) within the high-reflection coatings of the Advanced LIGO, Advanced Virgo and KAGRA gravitational-wave detectors: refractive index, thickness, optical absorption, composition, density, internal friction and elastic constants have been measured; the impact of deposition rate and post-deposition annealing on coating internal friction has been assessed. For Ta_2O_5 and SiO_2 layers, coating internal friction increases with the deposition rate, whereas the annealing treatment either erases or largely reduces the gap between samples with different deposition history. For Ta_2O_5–TiO_2 layers, the reduction of internal friction due to TiO_2 doping becomes effective only if coupled with annealing. All measured samples showed a weak dependence of internal

[5] Author to whom any correspondence should be addressed.
[6] Deceased, August 2018.
[7] Current affiliation: ENS de Lyon, CNRS, Laboratoire de Physique, Université de Lyon, Université Claude Bernard Lyon 1, F-69342 Lyon, France.
*This article is dedicated to the memory of L Balzarini.

Content from this work may be used under the terms of the Creative Commons Attribution 4.0 licence. Any further distribution of this work must maintain attribution to the author(s) and the title of the work, journal citation and DOI.

friction on frequency [$\phi_c(f) = af^b$, with $-0.208 < b < 0.140$ depending on the coating material considered]. SiO_2 films showed a mode-dependent loss branching, likely due to spurious losses at the coated edge of the samples. The reference loss values of the Advanced LIGO and Advanced Virgo input (ITM) and end (ETM) mirror HR coatings have been updated by using our estimated value of Young's modulus of Ta_2O_5–TiO_2 layers (120 GPa) and are about 10% higher than previous estimations.

Keywords: gravitational-wave detectors, thin films, internal friction, thermal noise

(Some figures may appear in colour only in the online journal)

1. Introduction

On September 14, 2015 at 09:50:45 UTC, a century after the fundamental predictions of Einstein [1, 2], the two detectors of the Advanced Laser Interferometer Gravitational-wave Observatory (Advanced LIGO) [3] simultaneously observed a transient gravitational-wave signal from the merger of two stellar-mass black holes [4]. This event was the first direct detection of gravitational waves and the first observation of a binary black hole merger, and marked the beginning of gravitational astronomy. Since then other detections followed [5], including a multi-messenger binary neutron-star merger [6, 7].

The Laboratoire des Matériaux Avancés (LMA) has provided the high-reflection (HR) and anti-reflective (AR) coatings for the core optics of the Advanced LIGO, Advanced Virgo [8] and KAGRA [9] gravitational-wave interferometers [10]. In such detectors, those large and massive suspended mirrors (up to $\varnothing = 35$ cm, $t = 20$ cm and $m = 40$ kg) play the crucial role of gravitational-field probes for the astrophysical signals [11].

The HR coatings are Bragg reflectors of alternate layers of ion-beam-sputtered (IBS) low- and high-refractive-index materials. Initially, tantalum pentoxide (Ta_2O_5, also known as *tantala*) and silicon dioxide (SiO_2, *silica*) had been chosen as high- and low-index materials, respectively, because of their low optical absorption at the typical wavelength of operation of the detectors ($\lambda_0 = 1064$ nm) [12]. Further development of the tantala layers was driven by thermal-noise issues.

In gravitational-wave interferometers, thermal noise arises from fluctuations of the mirror surface under the random motion of particles in coatings and substrates [13, 14]. Its intensity is determined by the amount of internal friction within the mirror materials, via the fluctuation-dissipation theorem [15]: the higher the mechanical-energy loss, the higher the thermal noise level. As the coating loss is usually several orders of magnitude larger than that of the substrate [16, 17], in the last two decades a considerable research effort has been committed to the investigation and the reduction of thermal noise in optical coatings.

Within the stack, tantala proved to be substantially more dissipative than silica [18, 19], making it the dominant source of coating loss. This loss was remarkably decreased by applying a titanium dioxide (TiO_2, *titania*) doping to tantala, a procedure developed by the LMA [20] for the LIGO Scientific Collaboration [21, 22]. Eventually, titania doping proved to be beneficial to the optical absorption of the HR coating as well, reducing it [23]. In the meantime, a technique to optimize the coating design in order to dilute the loss contribution of the high-index material had also been developed [24], further decreasing the resulting coating thermal noise [25].

In this paper, we report on the results of an extensive campaign of optical and mechanical characterization of the materials within the HR coatings of all the present kilometer-scale gravitational-wave interferometers. The relevance of these results is threefold: (i) we provide several parameters which are required to predict the coating thermal noise in the detectors; (ii) we point out the relevance of the synthesis process for the coatings' properties, in particular with respect to mechanical loss; (iii) we set reference values for further research and development of low-noise coatings.

2. Experiment

The amorphous IBS coating materials studied for this work are silica, tantala, titania and titania-doped tantala. They have been deposited with three different coaters at LMA: the custom-developed so-called *DIBS* and *Grand Coater* (GC) and a commercially available Veeco SPECTOR. The GC is used to coat the mirrors of gravitational-wave detectors. All coatings have been produced using accelerated, neutralized argon ions as sputtering particles. Argon was fed into the ion-beam sources while oxygen was fed into the chamber, for a total residual pressure inside the chamber of the order of 10^{-4} mbar. During deposition, the sputtered coating particles impinged on substrates heated up to about 100 °C. Other deposition parameters which may have had a relevant impact on the coating properties are the ion energy and current and the geometric configuration of the elements inside the chamber, i.e. the distances and the angles between the sputtering sources, the sputtered targets and the substrates to be coated. Each coater has its own specific set of values for these parameters, optimized for yielding the highest coating optical quality, resulting in a different deposition rate. However, in all the coaters the ion energy and current are of the order of 1 keV and 0.1 A, respectively.

The coatings have been deposited on different kind of substrates for different purposes: fused-silica witness samples ($\varnothing = 1''$, $t = 6$ mm) and silicon wafers ($\varnothing = 3''$, $t = 1$ mm) for the optical characterization, fused-silica disk-shaped resonators ($\varnothing = 50$ or 75 mm, $t = 1$ mm, with two parallel flats) for the mechanical characterization. Prior to coating deposition, to release the internal stress due to manufacturing and to induce relaxation, the fused-silica disks have been annealed in air at 900 °C for 10 h.

As part of the standard post-deposition process adopted for the production of gravitational-wave detectors' mirrors, in order to decrease both the internal stress and the optical absorption of the coatings, all the samples have been annealed in air at 500 °C for 10 h. This post-deposition annealing eventually turns out to be beneficial also for thermal noise, since it significantly decreases the coating loss.

2.1. Optical characterization

We measured the film refractive index and thickness, by transmission spectrophotometry through coated fused-silica witness samples and by reflection spectroscopic ellipsometry on coated silicon wafers.

Spectrophotometric measurements have been carried out with a Perkin Elmer Lambda 1050 spectrophotometer. Spectra have been acquired at normal incidence in the 400–1400 nm range. Film refractive index and thickness were first evaluated using the envelope method [26], then these results were used as initial values in a numerical least-square regression analysis. In the model, the adjustable parameters were the thickness and the (B_i, C_i) coefficients of the

Sellmeier dispersion equation:

$$n^2 = 1 + \sum_{i=1}^{3} \frac{B_i \lambda^2}{\lambda^2 - C_i}. \tag{1}$$

We used used two J.A. Woollam Co. instruments for the ellipsometric analysis, a VASE for the 190–1100 nm range and an M-2000 for the 245–1680 nm range. The wide wavelength range swept with both ellipsometers allowed us to extend the analysis from ultraviolet to infrared (0.7–6.5 eV). The optical response of the substrates has been characterized with prior dedicated measurements. To maximize the response of the instruments, coating spectra have been acquired for three different angles of incidence of the light ($\theta = 50°, 55°, 60°$), chosen to be close to the Brewster angle of each coating material ($\theta_B \sim 55°$ for silica and $\sim 64°$ for tantala, for instance). The refractive index and thickness of the films have been derived by comparing the experimental data with simulations based on realistic optical models [27] describing the properties of amorphous oxides, the Tauc–Lorentz [28] and Cody–Lorentz [29] models, providing a Kramers–Kronig-consistent determination of the complex refractive index. More details about our ellipsometric analysis can be found in a dedicated article [30].

Finally, we measured the coating optical absorption at $\lambda_0 = 1064$ nm through photo-thermal deflection [31].

2.2. Mechanical characterization

To measure the coating mass, we have used an analytical balance and measured the mass of the disks before and after the deposition, as well as after the annealing. To estimate the surface area coated in the deposition process, we have measured the diameter and the flat spacing of the disks with a Vernier caliper. As the coating thickness was known with high accuracy from the optical characterization, the coating density ρ_c could be straightforwardly estimated as the mass-to-volume ratio.

To measure the coating loss, we have applied the ring-down method [32] to the disks and measured the ring-down time of their vibrational modes. In each sample, for the kth mode of frequency f_k and ring-down time τ_k, the measured loss is $\phi_k = (\pi f_k \tau_k)^{-1}$. The coating loss ϕ_k^c can be written

$$\phi_k^c = \left[\phi_k + (D_k - 1)\phi_k^s \right] / D_k, \tag{2}$$

where ϕ_k^s is the measured loss of the bare substrate. D_k is the *dilution factor*, defined as the ratio of the elastic energy of the coating, E_c, to the elastic energy of the coated disk, $E = E_c + E_s$, where E_s is the elastic energy of the substrate. This ratio actually depends on the mode shape, which in turn is determined by the number of r radial and a azimuthal nodes [33], r and a respectively, denoted by the pair $(r, a)_k$. D_k is thus mode-dependent and can be written as a function of the frequencies f_k^s, f_k and of the masses m^s, m of the sample before and after the coating deposition, respectively [34]:

$$D_k = 1 - \left(\frac{f_k^s}{f_k} \right)^2 \frac{m^s}{m}. \tag{3}$$

We have used a gentle nodal suspension (GeNS) [35] to suspend the disks from the center, in order to avoid systematic damping from suspension. The system was placed inside a vacuum enclosure at $p \leqslant 10^{-6}$ mbar to prevent residual-gas damping. We have measured up to 16 modes on each disk, sampling the coating loss in the 1–30 kHz band. This sampling partially

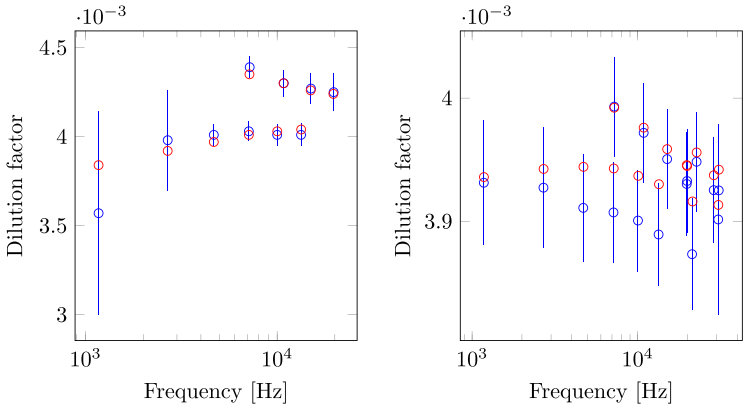

Figure 1. Comparison between measured (blue) and least-squares simulated (red) dilution factors, for Ta_2O_5 (left) and SiO_2 (right) coatings annealed in air at 500 °C during 10 h.

overlaps with the detection band of ground-based gravitational-wave interferometers (10–10^4 Hz).

For each coated disk, we have estimated the Young's modulus Y_c and the Poisson's ratio ν_c of the coating materials by adjusting finite-element simulations to match the measured dilution factors from equation (3): we found the set of values (Y_c, ν_c) minimizing the least-squares figure of merit

$$m_D = \sum_k \left[\frac{D_k^{\text{meas}} - D_k^{\text{sim}}}{\sigma_k^{\text{meas}}} \right]^2, \tag{4}$$

where D_k^{sim} and ($D_k^{\text{meas}} \pm \sigma_k^{\text{meas}}$) are the simulated and measured dilution factors, respectively (σ_k^{meas} is the measurement uncertainty). In this method, knowledge of the substrate parameters is critical: dimensions have been assigned measured values, values of density ($\rho = 2202$ g cm^{-3}), Young's modulus ($Y = 73.2$ GPa) and Poisson's ratio ($\nu = 0.17$) have been taken from the literature [36]; in a dedicated subset of simulations of the bare substrates, thickness t has been adjusted to minimize a merit function m_t of the same form as equation (4) for simulated and measured mode frequencies (f_k^{sim} and f_k^{meas}, respectively). For a few disks, we independently measured t with a micrometer and found that the discrepancy with the fitted values is less than 2%. Figure 1 shows the results of the overall process, comparing measured and least-squares simulated dilution factors of representative samples of tantala and silica. Dilution factors of modes with a different number of radial nodes lie on distinct curves, which we have called *mode families*; thus, for example, modes with $(0, a)_k$ and modes with $(1, a)_k$ belong to two different families (called *butterfly* and *mixed* modes, respectively). For a given substrate with (Y, ν), dilution factors are determined by the coating elastic constants: their average value depends on the Y_c/Y ratio, as in the case of flexural modes of cantilevers [37], whereas the separation between mode families increases as the difference $|\nu_c - \nu|$ grows.

Further details about our GeNS system and finite-element simulations are available elsewhere [38].

Table 1. Refractive index of coating materials of Advanced LIGO, Advanced Virgo and KAGRA.

	1064 nm	1550 nm
Ta_2O_5	2.05 ± 0.01	2.03 ± 0.01
Ta_2O_5–TiO_2	2.09 ± 0.01	2.08 ± 0.01
SiO_2	1.45 ± 0.01	1.45 ± 0.01

Table 2. Mechanical parameters of coating materials of Advanced LIGO, Advanced Virgo and KAGRA.

	ρ_c (g cm^{-3})	a (10^{-4} rad Hz^{-b})	b	Y_c (GPa)	ν_c
Ta_2O_5	7.33 ± 0.06	1.88 ± 0.06	0.101 ± 0.004	117 ± 1	0.28 ± 0.01
Ta_2O_5–TiO_2	6.65 ± 0.07	1.43 ± 0.07	0.109 ± 0.005	120 ± 4	0.29 ± 0.01
SiO_2	2.20 ± 0.04	0.20 ± 0.04	0.030 ± 0.024	70 ± 1	0.19 ± 0.01

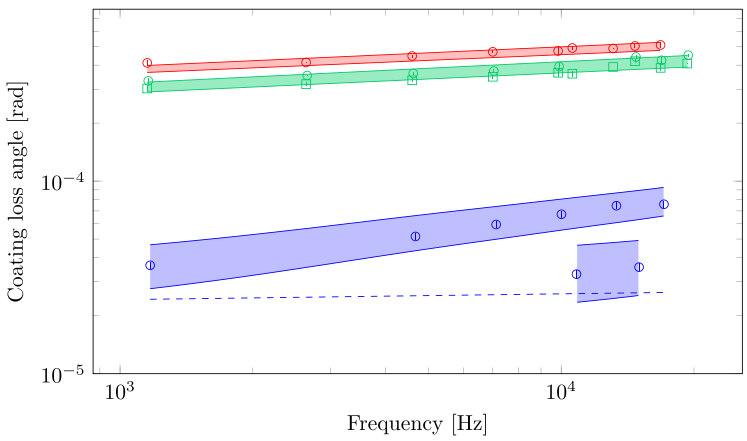

Figure 2. Mechanical loss of coating materials of Advanced LIGO, Advanced Virgo and KAGRA after annealing: Ta_2O_5 (red), Ta_2O_5–TiO_2 (green), SiO_2 (blue). Different markers denote distinct samples; error bars are shown, though barely visible. Shaded regions represent uncertainties from fitting a frequency-dependent loss model to each data set: $\phi_c(f) = af^b$ via least-squares linear regression for Ta_2O_5 and Ta_2O_5–TiO_2, $\phi_c(f) = af^b + \epsilon d\phi_e$ via numerical non-linear regression for SiO_2; the dashed curve shows the behavior of the af^b term only for SiO_2.

3. Results

In order to stress the impact of deposition parameters and post-deposition annealing, each coating material is discussed separately in the following.

Because of their relevance, results of coatings materials of gravitational-wave interferometers are summarized separately in (tables 1 and 2 and in figure 2).

Values of density, Young's modulus and Poisson's ratio are given with a standard deviation uncertainty, calculated from best-fit values of different samples. To characterize the loss behavior, we have fitted a frequency-dependent model $\phi_c(f) = af^b$ to the data of tantala, titania and titania-doped tantala coatings by linear regression; for silica coatings, in order to account

for the observed loss branching, an additional term $\epsilon d\phi_e$ [39] had to be included in the model ($\phi_c(f) = af^b + \epsilon d\phi_e$) and numerical non-linear regression has been used. This term quantifies the amount of spurious loss ϕ_e at the coated disk edge.

We observed a discrepancy between the results of spectrophotometry and ellispometry of less than 3%, though still larger than the respective uncertainties of the instruments. A possible explanation is that the optical response of the substrates has been systematically characterized only for the ellipsometric measurements. Moreover, the wavelength range swept with the ellipsometers was larger than that of photometric acquisitions, thus allowing for a better resolution of refractive index and thickness. While this discrepancy will be the subject of further investigation, only ellipsometric values are reported hereafter (unless otherwise explicitly mentioned). Refractive index is given for $\lambda_0 = 1064$ nm, as well as for the alternative wavelength $\lambda = 1550$ nm of future detectors such as the Einstein Telescope [40, 41] and Cosmic Explorer [42].

Upon annealing, the optical absorption of all the coatings (except for the crystallized TiO_2) decreased to sub-ppm (parts per million) values, which corresponds to an extinction coefficient of $10^{-7} < k < 10^{-6}$.

3.1. Ta_2O_5

Before annealing, the tantala films had similar refractive index (table 3) and equal Young's modulus and Poisson's ratio, whereas their density and loss were different (table 4 and figure 3).

Interestingly, the loss seems to be related to the coating deposition rate, determined by the energy and the flux of particles of the sputtering beam and by the configuration of the coating chamber. Whereas we found no correlation between the loss values and the distances of targets and substrates, the GC provided the slowest rate and lowest loss, the SPECTOR the fastest rate (3 Å s^{-1}) and the highest loss; thus, according to our results, the faster the deposition rate, the higher the loss.

The situation changed radically after the annealing, when all the films exhibited equal and significantly lower loss, as if their deposition history had been completely erased. This outcome seems to suggest that 500 °C in-air annealing for 10 h brings the structure of tantala coatings down to a stable optimal configuration for lowest loss, in agreement with observations that higher annealing temperatures or longer duration do not decrease loss further [43]. The coating structure depends on the chemical composition of the sputtered particles and on their energy distribution and electrical charge, however so far there is no model available nor there are any measurements for any of our coaters about these data. A research project has been recently funded to address this issue (project ViSIONs, Grant No. ANR-18-CE08-0023-01 of the French Government operated by the National Research Agency, ANR). The same *erasing effect* was observed later on in an independent experiment, where sputtered tantala coatings (IBS, magnetron) had been annealed after being deposited on heated substrates [44].

Finally, refractive index and density also slightly decreased after annealing, as the physical thickness of all the films increased.

By now, there have been many experimental studies on the internal friction of tantala coatings [18, 20, 23, 25, 34, 45–47]. However, the comparison with our results is not straightforward: previous works used coatings deposited with different conditions [25, 45] and/or stacked with other layers [18, 25, 46]; moreover, their analyses relied on assumptions made on the value of the coating Young's modulus [18, 20, 23, 34, 45–47]. Probably, the fairest comparison would be with annealed tantala coatings deposited with the GC on cantilever blades [20] under identical conditions, featuring a constant loss of $(3.0 \pm 0.1) \times 10^{-4}$ rad in the 60–1100 Hz band; by extrapolating our results of the annealed samples to lower frequencies, we obtain $(2.8 \pm 0.1) \times 10^{-4}$ rad at 60 Hz and $(3.8 \pm 0.2) \times 10^{-4}$ rad at 1100 Hz, matching the value from

Table 3. Refractive index of Ta_2O_5 films from different coaters.

	As deposited		Annealed 500 °C	
	1064 nm	1550 nm	1064 nm	1550 nm
GC	2.07 ± 0.01	2.06 ± 0.01	2.05 ± 0.01	2.03 ± 0.01
DIBS[a]	2.06 ± 0.01	2.04 ± 0.01	2.03 ± 0.01	2.02 ± 0.01
SPECTOR	2.11 ± 0.01	2.09 ± 0.01	2.09 ± 0.01	2.07 ± 0.01

[a] Measured only with a spectrophotometer.

Table 4. Mechanical parameters of Ta_2O_5 films from different coaters.

		ρ_c (g cm^{-3})	a (10^{-4} rad Hz^{-b})	b	Y_c (GPa)	ν_c
GC		7.40 ± 0.03	4.61 ± 0.11	0.036 ± 0.003	121 ± 1	0.30 ± 0.01
DIBS		7.04 ± 0.09	8.20 ± 0.24	—	117 ± 1	0.27 ± 0.01
SPECTOR		7.75 ± 0.03	7.60 ± 0.21	0.045 ± 0.003	121 ± 1	0.29 ± 0.01
GC	500 °C	7.33 ± 0.06	1.88 ± 0.06	0.101 ± 0.004	117 ± 1	0.28 ± 0.01
DIBS	500 °C	6.94 ± 0.09	2.27 ± 0.14	0.078 ± 0.007	115 ± 1	0.28 ± 0.01
SPECTOR	500 °C	7.47 ± 0.09	2.29 ± 0.06	0.079 ± 0.003	121 ± 2	0.29 ± 0.01

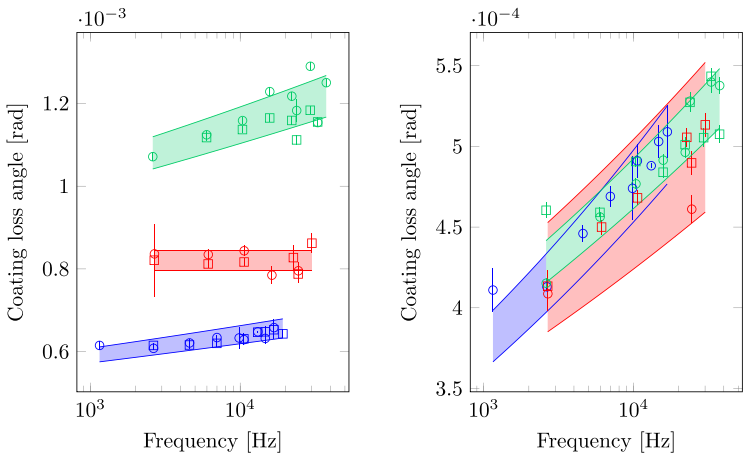

Figure 3. Mechanical loss of Ta_2O_5 films from different coaters: GC (blue), DIBS (red) and SPECTOR (green), before (left) and after the annealing (right). Different markers denote distinct samples; shaded regions represent uncertainties from fitting a frequency dependent loss model $\phi_c = af^b$ to each data set, via least-squares linear regression.

cantilever blades at 110 Hz. By correcting the cantilever blades results by our value of coating Young's modulus we would obtain 3.9 $\times 10^{-4}$ rad, so that the match with our results would be shifted to 1260 Hz. At 8.9 kHz, our results also match the value of $(4.7 \pm 0.6) \times 10^{-4}$ rad from quadrature-phase interferometry [34] on our SPECTOR films, obtained assuming constant loss but with no further assumptions on the coating Young's modulus; as a matter of fact, those results already pointed to an actual Young's modulus of 118 GPa, very close to our value (121 ± 2 GPa).

Table 5. Refractive index of the as-deposited TiO_2 film.

	1064 nm	1550 nm
GC	2.35 ± 0.05	2.33 ± 0.03

Table 6. Mechanical parameters of the TiO_2 film.

		ρ_c (g cm^{-3})	a (10^{-4} rad Hz^{-b})	b	Y_c (GPa)	ν_c
GC		3.89 ± 0.06	2.05 ± 0.16	0.140 ± 0.008	145 ± 1	0.26 ± 0.01
GC	500 °C	—	0.46 ± 0.05	0.330 ± 0.011	—	—

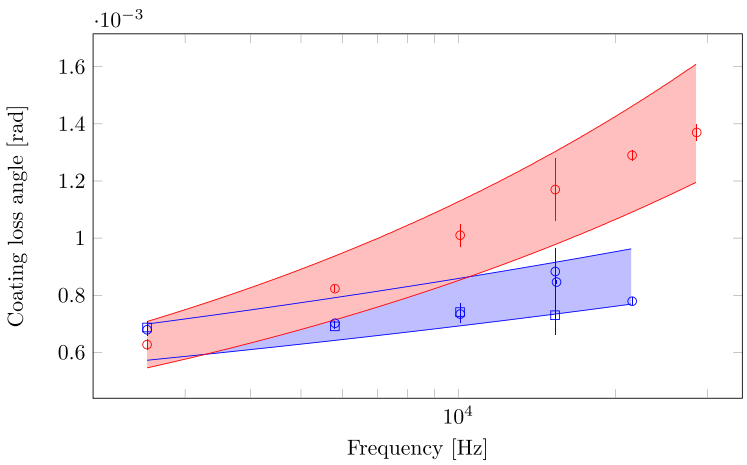

Figure 4. Mechanical loss of the TiO_2 film, before (blue) and after annealing (red). Different markers denote distinct samples; shaded regions represent uncertainties from fitting a frequency-dependent loss model $\phi_c = af^b$ to each data set, via least-squares linear regression.

If measured via nano-indentation, the Young's modulus of IBS tantala coatings appears to be about 140 GPa [48, 49], i.e. about 18% higher than our value. This difference could be explained by the nature of the films, deposited with different conditions, and by the fact that results from nano-indentation are model dependent and rely on assumptions about the coating Poisson's ratio. Furthermore, nano-indentations of the same coating deposited on different substrates might give different results: our tantala SPECTOR coatings yielded a reduced coating Young's modulus of 130 ± 3 GPa on silica witness samples and of 100 ± 3 GPa on silicon wafers.

3.2. TiO_2

Titania features a very high refractive index ($n \sim 2.3$, table 5), making it particularly well suited to increase the index contrast within the HR stack and thus consequently to allow for thinner high-index dissipative layers. Unfortunately, it becomes poly-crystalline when annealed at $T \geqslant 300$ °C [50, 51], yielding scattering and absorption losses far from meeting the stringent

Table 7. Refractive index of the Ta_2O_5–TiO_2 film with Ti/Ta = 0.27.

	As deposited		Annealed 500 °C	
	1064 nm	1550 nm	1064 nm	1550 nm
GC	2.11 ± 0.01	2.10 ± 0.01	2.09 ± 0.01	2.08 ± 0.01

Table 8. Mechanical parameters of the Ta_2O_5–TiO_2 film with Ti/Ta = 0.27.

		ρ_c (g cm^{-3})	a (10^{-4} rad Hz^{-b})	b	Y_c (GPa)	ν_c
GC		6.87 ± 0.06	4.82 ± 0.18	0.029 ± 0.004	122 ± 1	0.30 ± 0.01
GC	500 °C	6.65 ± 0.07	1.43 ± 0.07	0.109 ± 0.005	120 ± 4	0.29 ± 0.01

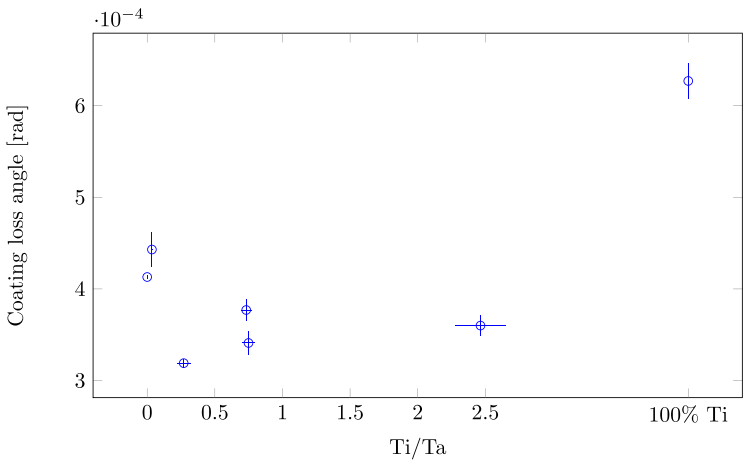

Figure 5. Mechanical loss of annealed Ta_2O_5–TiO_2 films deposited with the GC, as a function of the mixing ratio Ti/Ta; the data point of poly-crystalline TiO_2 is also shown, for comparison. For clarity, only values measured at ∼ 2.5 kHz are shown; the same trend has been observed at ∼ 10 kHz.

requirements of current gravitational-wave detectors [10]. Because of crystallization, we could not measure its refractive index and some mechanical parameters after annealing.

Before annealing, the density of our film (table 6) is slightly higher than that of typical sputtered titania films [52] and close to that of the crystalline anatase phase (3.9 g cm^{-3}). The loss increases significantly after the annealing, very likely due to crystallization (figure 4).

3.3. Ta_2O_5–TiO_2 mixture

The titania content in HR coatings for gravitational-wave detectors was initially determined by analyzing a set of Bragg reflectors with $\lambda/4$ layers [22], produced in the DIBS and in the GC with different titania-to-tantala mixing ratios; Ti/Ta = 0.27 yielded minimum loss and had thus been chosen as the optimal ratio. Since then, the design of the HR coatings of Advanced LIGO and Advanced Virgo has evolved [10, 38], while the Ti/Ta ratio in the titania-doped tantala layers remained the same. This choice is now confirmed by our latest loss measurements of single titania-doped tantala films produced with the GC, which we also characterized through

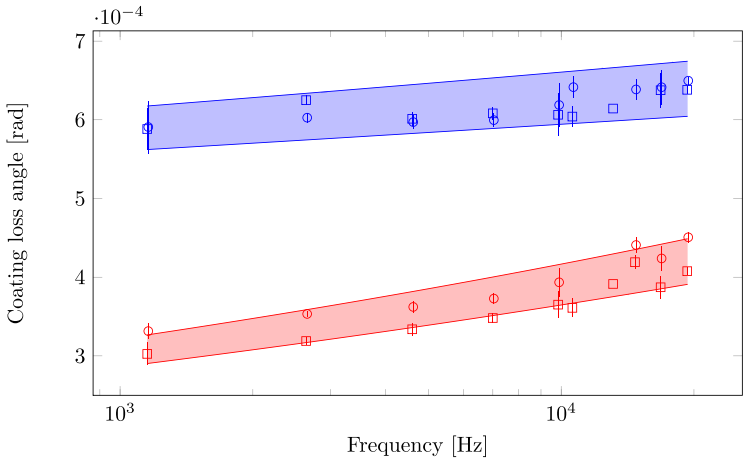

Figure 6. Mechanical loss of the Ta_2O_5–TiO_2 film with Ti/Ta = 0.27, before (blue) and after annealing (red). Different markers denote distinct samples; shaded regions represent uncertainties from fitting a frequency dependent loss model $\phi_c = af^b$ to each data set, via least-squares linear regression.

Rutherford back-scattering (RBS) and energy-dispersive x-ray (EDX) spectrometry (tables 7 and 8 and figures 5 and 6).

By comparing Ti/Ta = 0.27 titania-doped tantala to undoped GC tantala, we observe that both coating materials feature similar loss before annealing, whereas after annealing the loss of titania-doped tantala is $\sim 25\%$ lower in the whole sampled band, suggesting that the lower loss of titania-doped tantala is the result of a combined effect of mixing and annealing. The $\sim 25\%$ loss reduction has been confirmed by independent coating thermal noise measurements [53]. Except for the sample with Ti/Ta = 0.04, all the annealed titania-doped tantala coatings showed a lower loss than that of annealed undoped tantala; this is in fairly good agreement with molecular dynamics simulations showing that even small amounts of doping could decrease the coating internal friction [54].

Several results of mechanical loss measurements are already available for titania-doped tantala coatings [20, 21, 23, 25, 38, 46, 55, 56], and a correlation between coating internal friction and microscopic structure has also been found [57].

The fairest comparison with our results would be with annealed titania-doped tantala coatings deposited with the GC on cantilever blades [38] under identical conditions (deposition rate, Ti/Ta ratio), featuring a constant coating loss of $(2.4 \pm 0.3) \times 10^{-4}$ rad in the 50–900 Hz band; by extrapolating our results of the annealed samples to lower frequencies, we obtain $(2.2 \pm 0.1) \times 10^{-4}$ rad at 50 Hz and $(3.0 \pm 0.2) \times 10^{-4}$ rad at 900 Hz, matching the value from cantilever blades at 120 Hz. By correcting the cantilever blade results by our value of coating Young's modulus we would obtain 3.01×10^{-4} rad, so that the match with our results would be shifted to 920 Hz.

The refractive index of the Ta_2O_5–TiO_2 coating with Ti/Ta = 0.27 is in between those of tantala and titania, as expected [50]. Its optical absorption is lower than that of tantala, as we could measure on single films as well as on the HR coatings of Advanced LIGO and Advanced Virgo [10]; this in agreement with our previous measurements [23] and with previous studies of coatings deposited in similar conditions [50], showing that the lowest absorption is obtained with low titania content.

The annealing increased the physical thickness of the coating, which in turn resulted in a decrease of density and of refractive index, as demonstrated by previous studies as well [50]. Finally, we observed that the crystallization temperature is the same of that of tantala, i.e. between 600 °C and 650 °C [43], and hence much higher than that of titania [50, 51].

3.4. SiO_2

During the mechanical characterization of silica coatings, we observed a branching of the coating loss as a function of mode shape, closely following a separation in mode families (figure 7). This loss branching might be caused by a spurious contribution coming from the edge of the disks [39], which was also coated during deposition (masking the edge would have induced uncontrolled, undesired shadowing effects on the main surfaces). Such *edge effect* might be included in the frequency-dependent coating loss model by introducing an additional term $\epsilon d\phi_{\mathrm{e}}$, where ϕ_{e} is a constant edge energy loss, ϵ is a mode-dependent dilution factor linear density (with dimensions of m^{-1}) and d is the effective thickness of the coating deposited at the disk edge, so that the coating loss of silica can be written

$$\phi_{\mathrm{c}}(f) = af^b + \epsilon d\phi_{\mathrm{e}}. \tag{5}$$

The dilution factor density ϵ is calculated for a homogeneous disk as the ratio of the elastic energy per unit length of the edge to the total elastic energy of the disk. ϵ increases as the mode order $(r, a)_k$ grows but is substantially larger for butterfly modes which mainly vibrate at the edge, so that in the end their actual loss is larger. More details about the formal definition of an edge term $\epsilon d\phi_{\mathrm{e}}$ are available elsewhere [39].

If neglected, the edge effect could lead to a poor estimation of coating loss; this is particularly evident for the GC and DIBS samples (tables 9 to 11), for which the af^b term is hidden by the overall measured trend. When considering the af^b term only, the loss of the GC and the DIBS samples appeared fairly constant ($b \sim 0$) before annealing, whereas the loss of the SPECTOR sample showed a weak decreasing trend ($b < 0$); after the annealing, the loss values of the SPECTOR and GC samples moved closer to those of the DIBS sample but kept their distinctive features. Indeed, once again, we observed that the SPECTOR sample had the fastest deposition rate (2 Å s^{-1}) and the highest loss values; however, while having the same deposition rate (within 25% experimental uncertainty) than the GC sample, the DIBS sample had the lowest loss values. This result might be related to the unusually small measured density value for the DIBS sample, and will be subject to further investigation.

Previous studies have been made of the loss [18, 20, 25, 38, 46, 58–60] and the elastic constants [48] of silica coatings. Recently we found a correlation between loss and microscopic structure, which holds for the silica coatings discussed here and for bulk fused silica as well [61].

We may compare our results with those obtained from clamped cantilever blades [38] and free-standing micro-cantilevers made of coatings [60], all produced in the GC under identical conditions. The cantilever blades yielded a constant coating loss of $(4.5 \pm 0.3) \times 10^{-5}$ rad in the 50–900 Hz band; by considering the af^b term only and extrapolating the GeNS results of the annealed sample to lower frequencies, we obtain $(2.2 \pm 0.7) \times 10^{-5}$ rad at 50 Hz and $(2.4 \pm 1.0) \times 10^{-5}$ rad at 900 Hz, eventually matching the value from cantilever blades only at very high frequency. In other words, there is an irreconcilable discrepancy between our latest results obtained with disks and a GeNS system and our previous results obtained with clamped cantilever blades. One reason for this discrepancy may be that the loss measured with clamped

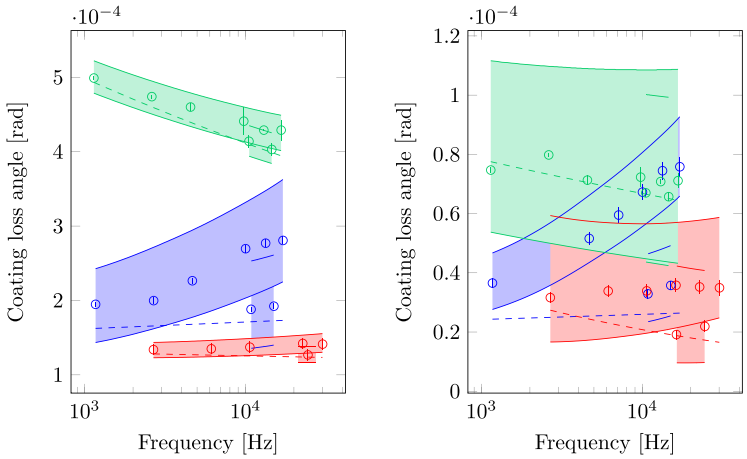

Figure 7. Mechanical loss of SiO_2 films from different coaters: GC (blue), DIBS (red) and SPECTOR (green), before (left) and after the annealing (right); shaded regions represent uncertainties from fitting a frequency-dependent loss model $\phi_c = af^b + \epsilon d\phi_e$ to each data set, via numerical non-linear regression; dashed curves show the behavior of the af^b term only.

Table 9. Refractive index of SiO_2 films from different coaters.

	As deposited		Annealed 500 °C	
	1064 nm	1550 nm	1064 nm	1550 nm
GC	1.47 ± 0.01	1.46 ± 0.01	1.45 ± 0.01	1.45 ± 0.01
DIBS[a]	1.44 ± 0.01	1.44 ± 0.02	1.44 ± 0.01	1.44 ± 0.02
SPECTOR	1.48 ± 0.01	1.47 ± 0.01	1.47 ± 0.01	1.46 ± 0.01

[a] Measured only with a spectrophotometer.

Table 10. Mechanical parameters of SiO_2 films from different coaters.

		ρ_c (g cm^{-3})	Y_c (GPa)	ν_c
GC		2.33 ± 0.06	66 ± 4	0.19 ± 0.02
DIBS		2.02 ± 0.09	74 ± 2	0.18 ± 0.02
SPECTOR		2.38 ± 0.01	78 ± 1	0.14 ± 0.01
GC	500 °C	2.20 ± 0.04	70 ± 1	0.19 ± 0.01
DIBS	500 °C	1.91 ± 0.09	75 ± 2	0.19 ± 0.02
SPECTOR	500 °C	2.36 ± 0.03	78 ± 1	0.11 ± 0.01

cantilever blades was affected by spurious suspension losses (in the clamp and/or in the weld [38]), yielding to its systematic overestimation. Another reason may be that the edge effect was not included in the analysis of the cantilevers, as it was unknown at that time. In principle, the edge effect might have affected the measurement of clamped cantilevers as well; however, it would have been hardly possible to isolate it anyway, as for cantilevers ϵ has the same value for all the flexural modes.

The free-standing micro-cantilevers had been measured before annealing, yielding a variable loss of $(0.8–1.8) \times 10^{-3}$ rad in the 1.2–21.8 kHz band [60]; again, by considering the af^b

Table 11. Mechanical loss of SiO_2 films from different coaters.

		a (10^{-4} rad Hz^{-b})	b	$d\phi_e$ (10^{-6} m)
GC		1.37 ± 0.22	0.024 ± 0.019	3.11 ± 0.26
DIBS		1.45 ± 0.06	-0.016 ± 0.005	0.39 ± 0.03
SPECTOR		8.87 ± 0.19	-0.083 ± 0.003	0.84 ± 0.11
GC	500 °C	0.20 ± 0.04	0.030 ± 0.024	1.41 ± 0.05
DIBS	500 °C	1.42 ± 0.54	-0.208 ± 0.044	0.42 ± 0.05
SPECTOR	500 °C	1.26 ± 0.23	-0.069 ± 0.024	0.19 ± 0.15

term only and extrapolating our GeNS results of the as-deposited sample to the same band, we obtain $(1.6 \pm 0.5) \times 10^{-4}$ rad at 1.2 kHz and $(1.7 \pm 0.5) \times 10^{-4}$ rad at 21.8 kHz, in clear disagreement with the results from free-standing micro-cantilevers. A likely explanation for this disagreement might be that the fabrication process of micro-cantilevers (with its steps of mask deposition, photolithography patterning and repeated etching [60]) may had changed the properties of the coating material they were made of. Otherwise, since in free-standing cantilevers the intrinsic stress is relieved (they only have a stress gradient along the thickness), this might be the first evidence of stress-dependent loss.

Remarkably, the SPECTOR sample is significantly denser and stiffer than the GC one, whose properties closely resemble those of bulk fused silica [36] (table 10).

3.5. HR coatings of Advanced LIGO and Advanced Virgo

The reference loss values of the Advanced LIGO and Advanced Virgo input (ITM) and end (ETM) mirror HR coatings (table 12) had been previously estimated [38] by assuming $Y_c =$ 140 GPa for titania-doped tantala layers [49]. These values may now be updated by using our measured value of Young's modulus of titania-doped tantala layers, $Y_c = 120$ GPa: the new estimations, listed in table 13, are about 10% higher than the previous ones [38] for both ITM and ETM coatings.

It is commonly accepted that the loss of an HR coating stack ϕ_{HR} is the linear combination of the measured loss of its constituent layers [18],

$$\phi_{HR} = \frac{t_H Y_H \phi_H + t_L Y_L \phi_L}{t_H Y_H + t_L Y_L}, \tag{6}$$

where t_H, Y_H and ϕ_H (t_L, Y_L and ϕ_L) are the thickness, the Young's modulus and the loss of the high-index Ta_2O_5–TiO_2 (low-index SiO_2) layers. Figure 8 shows the comparison between the expected loss of equation (6), calculated using the values of loss and Young's modulus of table 2, and the updated loss of table 13, obtained from direct loss measurements of the HR coatings [38]. The measured loss is fairly constant over the sampled band (2.7–22.4 kHz), whereas the expectations have the same frequency dependence of their dominant contribution, the titania-doped tantala layers. When extrapolating down to 0.1 kHz, i.e. the region of the Advanced LIGO and Advanced Virgo detection band limited by coating thermal noise, the expectations underestimate the actual measured loss of the HR coatings, by about 30% for the ITM coating and about 43% for the ETM coating. Though well-known [38], this discrepancy remains unexplained to date and will be subject to further investigation.

Table 12. Nominal specifications of Advanced LIGO and Advanced Virgo input (ITM) and end (ETM) mirror HR coatings: transmission T, number of layers N, thickness of titania-doped tanatala layers t_{H}, thickness of silica layers t_{L}, thickness ratio $r = t_{\mathrm{H}}/t_{\mathrm{L}}$, total thickness $t_{\mathrm{c}} = t_{\mathrm{H}} + t_{\mathrm{L}}$.

	T	N	t_{H} (nm)	t_{L} (nm)	r	t_{c} (nm)
ITM	1.4%	18	727	2080	0.32	2807
ETM	4 ppm	38	2109	3766	0.56	5875

Table 13. Mechanical loss of Advanced LIGO and Advanced Virgo input (ITM) and end (ETM) mirror HR coatings. $(r, a)_k$ is the pair denoting the kth mode with r radial and a azimuthal nodes, ϕ_k^{c} is the coating loss of the kth mode defined in equation (2).

	f (Hz)	$(r, a)_k$	ϕ_k^{c} (10^{-4} rad)	a (10^{-4} rad Hz^{-b})	b
ITM	2708.1	$(0,2)_1$	1.6 ± 0.1	1.1 ± 0.3	0.05 ± 0.03
	16 092.6	$(0,5)_{10}$	1.7 ± 0.1		
	16 283.9	$(1,2)_{12}$	1.8 ± 0.1		
	22 423.4	$(0,6)_{15}$	1.7 ± 0.1		
ETM	2708.6	$(0,2)_1$	2.4 ± 0.1	2.2 ± 0.6	0.01 ± 0.03
	6168.3	$(0,3)_4$	2.3 ± 0.1		
	16 088.1	$(0,5)_{10}$	2.5 ± 0.1		
	16 297.9	$(1,2)_{12}$	2.4 ± 0.1		
	22 414.5	$(0,6)_{15}$	2.3 ± 0.1		

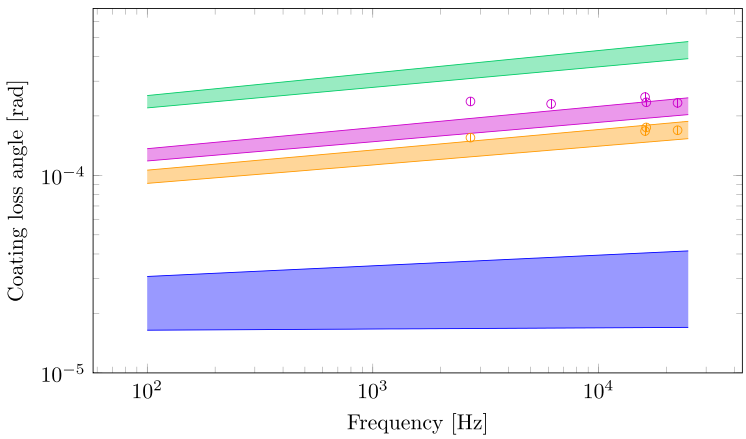

Figure 8. Mechanical loss of Advanced LIGO and Advanced Virgo input (ITM, orange) and end (ETM, purple) mirror HR coatings: comparison between the expected values (shaded regions) calculated via equation (6) and measured values (markers) from table 13. The frequency-dependent loss term $\phi_{\mathrm{c}}(f) = a f^b$ of Ta_2O_5–TiO_2 (green) and SiO_2 (blue) layers, from table 2, is also shown for comparison.

4. Conclusions

We presented in this work the results of an extensive campaign of optical and mechanical characterization of the IBS oxide layers (Ta_2O_5, TiO_2, Ta_2O_5–TiO_2, SiO_2) within the HR coatings of the Advanced LIGO, Advanced Virgo and KAGRA gravitational-wave detectors. These layers, deposited at the LMA, have been used for the first observing runs (designated O1 and O2) of Advanced LIGO and Advanced Virgo [62], when the first detections of mergers of black-hole and neutron-star binaries occurred.

Our measurements provide several coating parameters which are required to predict the power spectral density of coating thermal noise in gravitational-wave interferometers: refractive index, thickness, optical absorption, composition, density, internal friction and elastic constants have been measured; the mechanical parameters have been measured with a GeNS system [35], which has now been adopted as a standard apparatus by the Virgo and LIGO Collaborations [38, 63]. The main outcomes may be summarized as follows.

4.1. Frequency-dependent loss

Measurements of coating internal friction performed with our GeNS system [43, 64] showed weak but clear frequency-dependent trends, i.e. $\phi_c(f) = af^b$ with $-0.208 < b < 0.140$, depending on the sample considered; the frequency dependence observed for Ta_2O_5 and Ta_2O_5–TiO_2 layers has been later confirmed by independent measurements of coating thermal noise on the end mirror (ETM) HR coatings of Advanced LIGO and Advanced Virgo [53]. Our method for loss characterization is exclusively based on measured quantities (quality factors, frequencies and masses) and, unlike other experimental setups based on the ring-down method, does not require prior knowledge of the coating Young's modulus and thickness.

4.2. Deposition rate

With our tantala films, we observed that the level of coating internal friction is determined by the deposition rate: the slower the rate, the lower the loss; the same rule fairly holds for our silica films too. Thus, special care should be taken when comparing the loss of coating samples, even if composed of the same coating material.

4.3. Annealing

Post-deposition heat treatment makes the thickness increase and hence density decrease, while optical absorption, refractive index and internal friction decrease. Depending on the initial values considered, the reduction of internal friction is of a factor 1.5 to 2.5 for films Ta_2O_5, 1.8 for the Ta_2O_5–TiO_2 layer with Ti/Ta = 0.27, 5 to 6.5 for SiO_2 films. As the disks are annealed at 900 °C before deposition, the observed loss change upon 500 °C annealing is due to the coating only. Once annealed, all the Ta_2O_5 films exhibited equal loss, as if their deposition history had been erased, whereas the gap between the loss values of SiO_2 films decreased. For SiO_2 layers, it has been possible to establish a correlation between their structural change upon annealing and their internal friction [61]; for Ta_2O_5 and Ta_2O_5–TiO_2 films, we carried out analogous studies of structure and internal friction as a function of annealing temperature and duration [43, 65] but—despite the large variation of internal friction—we observed very limited structural change and eventually found no correlations.

4.4. Elastic constants

Our GeNS system allows the estimation of coating Young's modulus and Poisson's ratio, via the measurement of dilution factors [66]. Our values of Young's modulus for Ta_2O_5 and Ta_2O_5–TiO_2 coatings are 14% lower than those commonly accepted [48, 49] by the scientific collaborations running gravitational-wave interferometers. Two reasons may explain this discrepancy: likely the different nature of coating samples used in previous works, determined by the different deposition parameters used, and the method used, i.e. nano-indentations. The analysis of nano-indentation measurements relies on the prior knowledge of the coating Poisson's ratio and is model dependent. Moreover, nano-indentations of our tantala SPECTOR coatings suggest that the outcome of this technique may depend on the nature of the substrate: we obtained a reduced Young's modulus of 100 GPa from the coating sample deposited on a fused silica witness substrate, of 130 GPa from the coating sample deposited on a silicon wafer; both samples were from the same deposition run. While the discussion of the details about those measurements and their analysis is beyond the scope of this article, the important point we would like to stress here is that the outcomes of nano-indentations should be considered cautiously. Unlike nano-indentations, our estimation method is a non-destructive technique which does not require prior knowledge of the coating Poisson's ratio; it has been tested also on tantala SPECTOR coatings deposited at the same time on fused-silica disks and on silicon wafers, yielding consistent results. The agreement between finite-element simulations and measured dilution factors vouches for the reliability of our method; however, larger residuals for silica coatings seem to point out that either our model or our simulations might need further fine tuning, and will be be subject to further investigation.

4.5. Edge effect

SiO_2 films showed a mode-dependent loss branching, which may be accounted for by including a term of spurious loss from the coated disks' edge in the coating loss model, as it is already the case for bare substrates [39].

4.6. Loss of HR coatings

The reference loss values of the Advanced LIGO and Advanced Virgo input (ITM) and end (ETM) mirror HR coatings [38] have been updated by using our estimated value of Young's modulus of titania-doped tantala layers ($Y_c = 120$ GPa) and are about 10% higher than previous estimations. By using our latest measurements of SiO_2 and Ta_2O_5–TiO_2 films deposited on fused silica disks and the updated loss values of the Advanced LIGO and Advanced Virgo HR coatings, we demonstrated that the loss of an HR coating stack is not equal to the linear combination of the measured loss of its constituent layers: a different frequency dependence makes the linear combination smaller than the measured loss at lower frequencies (below 2 kHz). This is a confirmation of what had already been observed with the same coatings (deposited with the same conditions) measured on clamped cantilever blades [38].

4.7. Metrology issue

The frequency dependence of coating loss of Ta_2O_5, Ta_2O_5–TiO_2 and SiO_2 coatings had not been observed previously with clamped cantilever blades [20, 23, 38]. Our latest loss measurements of Ta_2O_5 and Ta_2O_5–TiO_2 layers are compatible with previous estimations at least in some specific frequency band, whereas in the case of SiO_2 coatings there is a discrepancy that might be explained by considering the presence of spurious suspension losses and of the edge effect in the clamped cantilevers.

5. Perspectives

The IBS oxide layers deposited at the LMA are now being used for the ongoing joint observing run (O3) of Advanced LIGO and Advanced Virgo [62] with the possible participation of KAGRA, which started on April 1, 2019. They will be used also for the following run (O4), in which KAGRA will fully join the present network of detectors.

Coating thermal noise is expected to be a severe limitation for present [3, 8] and future [40, 41] ground-based gravitational-wave interferometers. This is the reason why, in the context of a medium term plan to improve the design sensitivity of their detectors (the projects are called *A*+ and *Advanced Virgo*+), the LIGO and Virgo Scientific Collaborations have already planned to produce new sets of mirrors with lower coating thermal noise, to be used for the next observing run (O5).

More generally, coating thermal noise is already a fundamental limit for a large number of precision experiments based on optical and quantum transducers, such as opto-mechanical resonators [67], frequency standards [68] and quantum computers [69]. Thus, in the context of a world-wide research effort devoted to solve this issue, the development of low-thermal-noise amorphous optical coatings is a long-term activity of the LMA [70].

Besides lowering the temperature of the mirrors [9, 40–42], there are three key properties that may reduce coating thermal noise [17]: coating thickness and internal friction, which depend on intrinsic properties of coating materials, and laser beam size, which requires the development of deposition technology and larger substrates. Furthermore, the lowest coating thermal noise occurs when the coating Young's modulus is matched to that of the substrate [17]. Coating thickness is in turn a monotonically decreasing function of the refractive index contrast $c = n_{\mathrm{H}}/n_{\mathrm{L}}$ in the HR stack, where n_{H} and n_{L} are the high and low refractive indices, respectively; thus the larger c, the lower the coating thickness and hence the coating thermal noise (at constant reflection). As a consequence, the optimal coating materials would feature the lowest internal friction and the largest index contrast at the same time, a Young's modulus matching as much as possible that of the substrate to be coated (73.2 GPa in fused-silica substrates used for room-temperature operation, 130 to several hundreds of GPa in silicon or sapphire substrates for cryogenic operation) and, in order to limit thermal lens effects, an optical absorption at least as low as it is to date. By taking the results from Ta_2O_5–TiO_2 and SiO_2 coatings presented here as a reference (see tables 1 and 2), future low-thermal-noise coating layers should have $c > 1.44$, $\phi_{\mathrm{c}} < 2.4 \times 10^{-4}$ at 10^2 Hz and $k \sim 10^{-7}$ at $\lambda_0 = 1064$ nm or $\lambda = 1550$ nm.

Acknowledgments

The authors would like to thank C Bernard, S Gavarini and N Millard-Pinard of the Institut de Physique des 2 Infinis de Lyon for the RBS measurements and E Coillet for the data analysis; R Brescia, A Scarpellini and M Prato of the Istituto Italiano di Tecnologia for the EDX and XPS analyses; M Neri of the OPTMATLAB for the preliminary ellipsometric analysis; S Pavan and J-L Loubet of the Laboratoire de Tribologie et Dynamique des Systèmes for the nano-indentation analysis.

ORCID iDs

M Granata https://orcid.org/0000-0003-3275-1186
A Amato https://orcid.org/0000-0001-9557-651X

References

[1] Einstein A 1916 *Sitzungsber. K. Preuss. Akad. Wiss.* **1** 688
[2] Einstein A 1918 *Sitzungsber. K. Preuss. Akad. Wiss.* **1** 154
[3] Aasi J *et al* 2015 *Class. Quantum Grav.* **32** 074001
[4] Abbott B P *et al* 2016 *Phys. Rev. Lett.* **116** 061102
[5] Abbott B P *et al* 2019 *Phys. Rev.* X **9** 031040
[6] Abbott B P *et al* 2017 *Phys. Rev. Lett.* **119** 161101
[7] Abbott B P *et al* 2017 *Astrophys. J. Lett.* **848** L12
[8] Acernese F *et al* 2015 *Class. Quantum Grav.* **32** 024001
[9] Aso Y *et al* 2013 *Phys. Rev.* D **88** 043007
[10] Pinard L *et al* 2017 *Appl. Opt.* **56** C11
[11] Abbott B P *et al* 2016 *Phys. Rev. Lett.* **116** 131103
[12] Beauville F *et al* 2004 *Class. Quantum Grav.* **21** S935
[13] Saulson P R 1990 *Phys. Rev.* D **42** 2437
[14] Levin Y 1998 *Phys. Rev.* D **57** 659
[15] Callen H B and Greene R F 1952 *Phys. Rev.* **86** 702
[16] Crooks D R M *et al* 2002 *Class. Quantum Grav.* **19** 883
[17] Harry G M *et al* 2002 *Class. Quantum Grav.* **19** 897
[18] Penn S D *et al* 2003 *Class. Quantum Grav.* **20** 2917
[19] Crooks D R M *et al* 2004 *Class. Quantum Grav.* **21** S1059
[20] Comtet C *et al* 2007 Proc. 42nd Rencontres de Moriond on Gravitational Waves and Experimental Gravity (http://hal.in2p3.fr/in2p3-00177578)
[21] Harry G M *et al* 2006 *Appl. Opt.* **45** 1569
[22] Harry G M *et al* 2007 *Class. Quantum Grav.* **24** 405
[23] Flaminio R *et al* 2010 *Class. Quantum Grav.* **27** 084030
[24] Agresti J *et al* 2006 *Proc. SPIE* **6286** 628608
[25] Villar A E *et al* 2010 *Phys. Rev.* D **81** 122001
[26] Cisneros J I 1998 *Appl. Opt.* **37** 5262
[27] Fujiwara H 2007 *Spectroscopic Ellipsometry: Principles and Applications* (New York: Wiley)
[28] Jellison G Jr and Modine F 1996 *Appl. Phys. Lett.* **69** 371
[29] Ferlauto A *et al* 2002 *J. Appl. Phys.* **92** 2424
[30] Amato A *et al* 2019 *J. Phys. Mater.* **2** 035004
[31] Boccara A C *et al* 1980 *Opt. Lett.* **5** 377
[32] Nowick A and Berry B 1972 *Anelastic Relaxation in Crystalline Solids* (New York: Academic) pp 582–602
[33] McMahon G W 1964 *J. Acoust. Soc. Am.* **36** 85
[34] Li T *et al* 2014 *Phys. Rev.* D **89** 092004
[35] Cesarini E *et al* 2009 *Rev. Sci. Instrum.* **80** 053904
[36] McSkimin H J 1953 *J. Appl. Phys.* **24** 988
[37] Heptonstall A *et al* 2006 *Phys. Lett.* A **354** 353
[38] Granata M *et al* 2016 *Phys. Rev.* D **93** 012007
[39] Cagnoli G *et al* 2018 *Phys. Lett.* A **382** 2165
[40] Hild S *et al* 2011 *Class. Quantum Grav.* **28** 094013
[41] Abernathy M *et al* 2011 Einstein gravitational-wave Telescope conceptual design study *Technical note* ET-0106C-10 (https://tds.ego-gw.it/?content=3&r=8709)
[42] Abbott B P *et al* 2017 *Class. Quantum Grav.* **34** 044001
[43] Amato A *et al* 2018 *J. Phys.: Conf. Ser.* **957** 012006
[44] Vajente G *et al* 2018 *Class. Quantum Grav.* **35** 075001
[45] Martin I W *et al* 2010 *Class. Quantum Grav.* **27** 225020
[46] Principe M *et al* 2015 *Phys. Rev.* D **91** 022005
[47] Cesarini E *et al* 2011 *J. Non-Cryst. Solids* **357** 2005
[48] Çetinörgü E *et al* 2009 *Appl. Opt.* **48** 4536
[49] Abernathy M R *et al* 2014 *Appl. Opt.* **53** 3196
[50] Lee C-C *et al* 2006 *Appl. Opt.* **45** 9125
[51] Chen H-C *et al* 2008 *Appl. Opt.* **47** C284
[52] Bundesmann C *et al* 2017 *Appl. Surf. Sci.* **421** 331
[53] Gras S and Evans M 2018 *Phys. Rev.* D **98** 122001

[54] Trinastic J P *et al* 2016 *Phys. Rev.* B **93** 014105
[55] Martin I W *et al* 2008 *Class. Quantum Grav.* **25** 055005
[56] Martin I W *et al* 2009 *Class. Quantum Grav.* **26** 155012
[57] Bassiri R *et al* 2013 *Acta Mater.* **61** 1070
[58] Martin I W *et al* 2014 *Class. Quantum Grav.* **31** 035019
[59] Hamdan R *et al* 2014 *J. Chem. Phys.* **141** 054501
[60] Mariana S *et al* 2019 *Mater. Res. Express* **6** 045206
[61] Granata M *et al* 2018 *Phys. Rev. Mater.* **2** 053607
[62] Abbott B P *et al* 2018 *Living Rev. Relativ.* **21** 3
[63] Vajente G *et al* 2017 *Rev. Sci. Instrum.* **88** 073901
[64] Granata M *et al* 2016 *LIGO technical note* G1600641
[65] Coillet E 2017 Structural characterization of thin non-crystalline layers for low thermal noise optics *PhD Thesis* Université Claude Bernard Lyon 1 (https://tel.archives-ouvertes.fr/tel-01626513)
[66] Granata M *et al* 2015 *Arch. Metall. Mater.* **60** 365
[67] Aspelmeyer M *et al* 2014 *Rev. Mod. Phys.* **86** 1391
[68] Matei D G *et al* 2017 *Phys. Rev. Lett.* **118** 263202
[69] Martinis J M *et al* 2005 *Phys. Rev. Lett.* **95** 210503
[70] Granata M *et al* 2020 *Appl. Opt.* **59** A229